The effect of nickel on the mechanical behavior of molybdenum P/M steels

B.A. Gething[a], D.F. Heaney[a,*], D.A. Koss[a,b], T.J. Mueller[a]

[a] *The Center for Innovative Sintered Products, 118 Research Building West, The Pennsylvania State University, University Park, PA 16802, USA*

[b] *Department of Materials Science and Engineering, The Pennsylvania State University, University Park, PA, USA*

Abstract

This study has examined the effects of nickel alloying additions on the microstructural characteristics and mechanical properties of Fe–xNi–0.85Mo–0.4C-base steels that were powder processed using double-press double-sinter processing to maximize density. The steels were examined in the as-processed condition as well as in a quench-and-temper heat treated condition. Tensile behavior indicates that while nickel content (at levels of 2,4, and 6%) increased tensile strength in the as-sintered condition, it did not significantly affect tensile strength in the quenched and tempered condition. In both conditions increasing Ni content decreased elongation to fracture. The 4% Ni steel, which tended to have the smallest maximum pore size, also exhibited the greatest fatigue strength.
© 2004 Published by Elsevier B.V.

1. Introduction

For a powder metallurgy (P/M) component to be considered for high performance applications, porosity must be reduced to a minimum; i.e. density must be maximized. Many methods to reduce porosity have been explored, such as the hydropulsor technique [1], warm compaction [2], and high temperature sintering [3]. One of the more common methods to reduce porosity is known as "double-press double-sintering" (DPDS), which decreases bulk porosity of conventional ferrous-based components from approximately 10% after the conventional single-press single-sinter (SPSS) to 5% porosity after DPDS [4,5].

Another method to improve the mechanical properties of P/M materials is through the use of alloy additions. These additions can be pre-alloyed with the iron prior to powder production or added as an elemental powder addition to the base iron powder. For example, a "workhorse" series of alloys for moderate- to high-stress P/M applications are the P/M grades 4200, 4400 and 4600 series steels, which rely on nickel, carbon, and molybdenum additions. In most cases, the nickel and the carbon are added as elemental powder additions, whereas the molybdenum is pre-alloyed with the base iron powder. Due to the industrial importance of these PM steels, many studies have addressed aspects of their processing and behavior [2–13]. However, each study has used a slightly different alloy or processing method, and comparisons as well as standardized properties are difficult to ascertain. For example, while it is known that strength increases with an increase in nickel content [14], limited elongation data exists. Engstrom and Allroth reported that elongation moderately increases with nickel content, but at nickel contents greater than 6%, which are of lesser interest today [15]. Similarly, Morioka [7,8] examined fatigue strength for 2 and 4% nickel alloys, but each of these alloys had different molybdenum contents and the 4% nickel alloy also contained copper additions. No study has determined tensile and fatigue behavior as a function of nickel content while maintaining constant process and alloy parameters.

* Corresponding author. Tel.: +1 814 865 7346; fax: +1 814 863 8211
E-mail address: dfh100@psu.edu (D.F. Heaney).

The objective of this work is to examine the effect of nickel additions on the tensile and fatigue behavior of molybdenum P/M steels. High density processing was applied through DPDS to reduce the effects of porosity, thereby increasing performance and making the effects of the alloy additions more prominent. This study examines the influences of the nickel additions on porosity, microstructure, hardness, tensile strength, and elongation to fracture in both the as-sintered condition and a quenched-and-tempered heat-treated condition; fatigue strength at 10^6 cycles was also determined for the "heat-treated" condition.

2. Experimental procedure

Samples were fabricated from water-atomized alloy powder and elemental additions of nickel and carbon. If nickel and carbon are pre-alloyed with the base iron material, the compressibility is reduced resulting in lower overall density, while the molybdenum has little effect on the compressibility of the base iron powder. The base iron powder was Atomet 4401, supplied by Quebec Metal Powders Limited. Atomet 4401 is water-atomized, pre-alloyed iron powder consisting of 0.8% Mo and 0.16% Mn on a weight basis. The iron powder had a rounded but irregular shape with a mean powder particle size of 37 μm. The elemental nickel powder, Novamet Type 123, had a mean particle size of 8 μm and was spherical and sponge-like in appearance.

Carbon from Asbury Graphite Mills Inc., (PM 5) was added in the form of graphite. The initial admixed carbon amount was 0.46 wt.% which resulted in a nominal post-sintered composition of 0.40%. This reduction of 0.06% during sintering is believed to result from the carbon reduction of the oxide layer on the Atomet 4401 powder, and thus, the carbon content identified for the alloys in this study refers to post-sintered carbon content. Typically, prior studies often do not differentiate from pre- and post-sintered carbon content. It will be assumed that a pre-sintered carbon content of 0.5% in prior studies is comparable to the post-sintered 0.4% carbon content in the present study, as some decarburization during the sintering process is likely.

A lubricant, Acrawax "C," in the amount of 0.5 wt.% was also added to the alloy mixtures. A total of 100 g was mixed for each alloy in a Glen Mills Inc., turbula mixer for 30 min, with the rotation speed set at 50 rpm.

Two different geometries of samples for mechanical testing were used for the study. Standard P/M dog-bone tensile bars were powder processed to the MPIF Standard 10 geometry, with a thickness of approximately 0.65 cm. After sintering, the section for quenched and tempered specimens was reduced by machining to approximately half the original width. This modification increased the stress in the gage section to ensure fracture in the gauge section and to eliminate grip slippage, which was a problem in the unmodified samples. Four-point-bend fatigue bars were fabricated to the MPIF Standard 40 geometry, with a thickness of approximately 0.45 cm.

All samples were initially pressed at 550 MPa and subsequently pre-sintered in an Inconel Lindberg retort furnace by being heated to 450 °C at 5 °C/min and held for 180 min for lubricant burnout, then being heated to 750 °C at 10 °C/min and held for 30 min in flowing 10% hydrogen/90% nitrogen atmosphere to pre-sinter and anneal the samples, and then furnace cooled at a rate of approximately 15 °C/min. All samples were then pressed a second time at 825 MPa. A resizing die was used for the second pressing of the tensile specimens. The opening of the die was larger than the initial die by 0.127 mm in all directions, allowing for easier part entry to the die. The walls were tapered by the 0.127 mm over a distance of 1.27 cm so that the inside of the die was the same size as the initial die. Before the samples were pressed a second time, they were lightly sprayed with zinc stearate to reduce friction effects. High temperature sintering was performed in a CM 333 pusher furnace at a temperature of 1288 °C and a time of 60 min. A sintering atmosphere of 50% H_2 and 50% N_2 was used. Specimens were air cooled in the furnace cooling zone at an undetermined cooling rate.

After the double-press double-sinter processing, half of the samples from the study were heat treated by austenitizing at 870 °C (1600 F) at a 0.7% C potential in an endothermic atmosphere for 60 min and then quenched in oil. These samples were subsequently tempered for 60 min at 390 °C in an N_2 atmosphere. This temperature represents the upper range of temperatures used to temper high-strength powder-processed steels [3–12,16] in order to ensure that the specimens regained the maximum amount of tensile ductility.

The Archimedes technique was used to measure the density of all samples, while the percent porosity was measured using an AccuPyc 1330 pycnometer. Using this technique, samples were compacted and pre-sintered, then crushed into small fragments. These fragments were then measured for density using the pycnometer; this density was utilized as the theoretical density. Comparing this value to the Archimedes values yielded the percent porosity.

Hardness measurements were taken using an LR-Series Rockwell-Type hardness indenter. Both Rockwell "B" and "C" scale measurements were taken. Microhardness of individual steel phases was measured using a Leco M-400H-0 testing apparatus using a Vickers diamond indenter. The tensile strengths were measured using an Instron 4100 tensile tester, at a strain rate of 10^{-2} s.

Fatigue strength at 10^6 cycles was measured using the four-point-bend test fixture described above [17]. The fixture was equipped with pins that allow for two directions of articulation to minimize stress concentrations during testing. Fatigue testing was performed using a MTS 1036 Materials Testing machine under load control with a stress ratio (R) of 0.1. All samples were tested at a frequency of 30 Hz at ambient conditions. All specimens were surface conditioned to remove sharpness and imperfections along edges, minimizing stress risers that might cause inconsistent mechanical
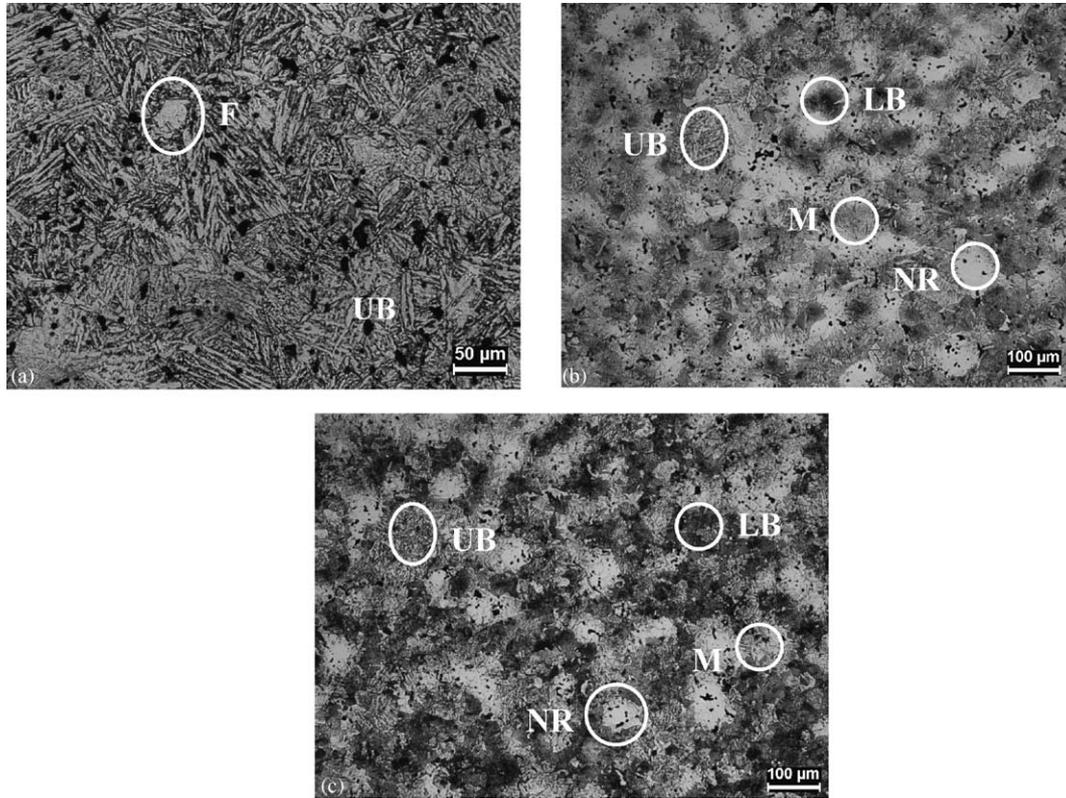
Fig. 1. Optical micrographs of as-sintered Fe–xNi–0.85Mo–0.4C steel containing (a) 2% Ni, (b) 4% Ni, and (c) 6% Ni. The microstructure designations are as follows: UB—upper bainite, F—pro-eutectoid ferrite, M—martensite, LB—lower bainite, and NR—Ni-rich retained austenite.

performance. Samples were placed in a vibratory polisher for 10 h. The polisher operates by vibrating samples and milling media together in a bell-shaped bowl. As these objects vibrate, they tumble onto one another, smoothing the surface and edges.

In order to determine the fatigue strength of materials at 10^6 cycles, a staircase method was employed [18]. For this procedure, the fatigue strength was first estimated based on prior results by Morioka [8], and the first test was run at this stress amplitude. If the specimen did not fail at this stress level, the next test was run at a higher level, and the converse was performed if the specimen failed. The test procedure continued in this fashion with stress levels being raised and lowered for sequential test specimens. Increments of 20 MPa, approximately 5% of the estimated fatigue strength, were used for all staircase tests, and approximately 15 specimens were tested for each condition to determine the average fatigue strength at 10^6 cycles in a statistically reliable manner. The average fatigue strength (S) was determined by using only the failure or survival specimens, depending on which had the smaller total. The mean fatigue strength and standard deviation (s) were calculated by using the following equations from Lipson and Sheth [18].

$$\bar{S} = S_0 + \left[\frac{A}{\sum n_i} \pm \frac{1}{2} \right] \tag{1}$$

$$s = 1.62d \left[\frac{B \sum n_i - A^2}{\sum (n_i)^2} + 0.029 \right] \tag{2}$$

In the above equations, S_0 is the lowest stress level during a particular staircase test, and d the interval spacing or difference of stress between two steps of the staircase. According to Lipson and Sheth, the value for d should not exceed 10% of S_0. A and B are parameters based on specimen responses. The stress levels are given coded scores i, where $i = 0$ for the lowest stress level, and n_i, is the number of failures (or survivals) for a given staircase test. In Eq. (1) "+1/2" is used if survivals are less frequent and "−1/2" if survivals are more frequent.

3. Results and discussion

3.1. Microstructural characteristics

The microstructures of several alloys were examined to determine the phases present in both the as-sintered and heat-treated conditions. In the as-sintered condition shown in Fig. 1a. the microstructure of the 2% Ni steel is primarily upper bainite (UB) (Vickers hardness value, HVN = 209) with small, discontinuous regions of randomly dispersed, soft (HVN = 139) regions believed to be pro-eutectoid ferrite (F).
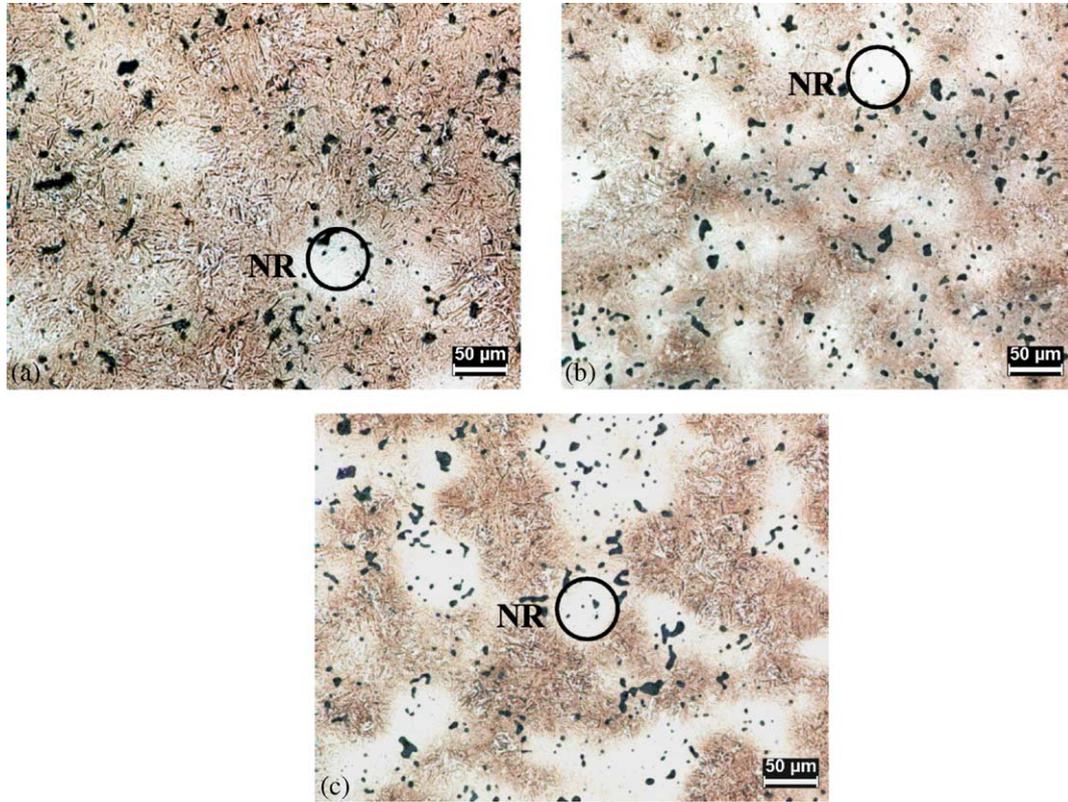
Fig. 2. Optical micrographs of quenched and tempered (a) 2% Ni alloy, (b) 4% Ni alloy, and (c) 6% Ni alloy. NR denotes regions that are primarily Ni-rich retained austenite.

The upper bainite regions are comparatively soft when compared to previous results [19]; this softening could be a result of tempering of the upper bainite region during the slow cooling process after sintering.

The microstructures of the 4% Ni and 6% Ni alloys in the as-sintered conditions, Fig. 1b and c, are similar to those observed by Kosko in a PM steel with similar composition [5], although no lamellar pearlite regions were observed in the present case. The microstructure also includes regions of upper bainite (UB) (HVN = 248) as well as lower bainite (LB) (HVN = 370) and areas of a needle-like, very hard (HVN = 575) martensite (M) phase. All three of these constituents appear to form in random locations. In addition, a soft (HVN = 180), nickel-rich austenite (NR) is also present; it contains many secondary pores that were formed when the nickel particles dissolved in the iron matrix. The regions of

hard martensite and bainite are more prevalent in the 6% Ni alloy.

After the quench-and-temper heat treatment, the microstructures of all three steels consist primarily of tempered martensite with minor levels of Ni-rich retained austenite; see Fig. 2. The amount of retained austenite phase increases with increasing Ni content, as expected.

The average porosity values were determined from five replicates of each alloy, and the results are shown in Tables 1 and 2. Both the green and DPDS porosity levels were the highest for the 6% Ni alloy, lowest for the 4% Ni, and intermediate for the 2% Ni alloy. One would expect a decrease in porosity of the alloy as the nickel content is increased since the nickel powder is finer and would be more prone to sinter densification. On the other hand, densification

Table 1
Green and sintered densities of (Fe–xNi) alloys investigated in this study (error is standard deviation)

Alloy	Green porosity (%)	DPDS porosity (%)	Densification
(Fe–2Ni)–0.85Mo–0.4C	10.62 ± 0.05	3.57 ± 0.01	7.05 ± 0.06
(Fe–4Ni)–0.85Mo–0.4C	10.93 ± 0.06	3.24 ± 0.02	7.69 ± 0.08
(Fe–6Ni)–0.85Mo–0.4C	11.62 ± 0.05	3.79 ± 0.02	7.83 ± 0.07

Table 2
Mechanical properties of Fe–*x*Ni steels investigated in this study (error is standard deviation)

Alloy	Hardness	Tensile strength (MPa)	Elongation (%)	Fatigue strength at 10^6 cycles
As-sintered properties				
(Fe–2Ni)–0.85Mo–0.4C	81±2 (HRB)	642 ± 8	8.7 ± 0.5	
(Fe–4Ni)–0.85Mo–0.4C	99±3 (HRB)	760 ± 24	6.2 ± 0.7	
(Fe–6Ni)–0.85Mo–0.4C	108±3 (HRB)	943 ± 21	5.0 ± 0.9	
Quenched-and-tempered properties				
(Fe–2Ni)–0.85Mo–0.4C	48 ± 1 (HRC)	1530 ± 14	1.9 ±0.1	373 ± 6
(Fe–4Ni)–0.85Mo–0.4C	48 ±1 (HRC)	1551 ± 27	0.9 ± 0.2	396 ± 26
(Fe–4Ni)–0.85Mo–0.4C	49 ± 1 (HRC)	1579 ± 25	0.8 ± 0.2	361 ± 19

of the cold-pressed compact during DPDS decreases with increasing amounts of Ni, as also observed elsewhere [20]. Thus, steels with low Ni additions have high compressibility but low densification, and high-Ni-content steels have low compressibility with high densification, as shown in Table 2. The result is the 4% Ni alloy exhibiting the lowest amount of final porosity, possessing both adequate compressibility and densification.

3.2. Mechanical properties: tensile behavior

As indicated in Table 2, increasing Ni content causes an increase in both the hardness and tensile strength in the *as-sintered* condition. For example, tensile strength increases from 642 to 943 MPa as Ni content increases from 2% to 6%. The increasing strength and hardness of alloys with higher Ni content results in a subsequent decrease in elongation for these alloys; tensile elongation is highest at 2% Ni (8.7%), and decreases to 5.0% at 6% Ni content.

In contrast to the behavior in the as-sintered condition, Ni content has only a minor effect on the hardness and tensile strength in the *quenched and tempered* condition with all three alloys having tensile strength of ≈1550 MPa; see Table 2. The 2% Ni alloy exhibits the highest elongation at 1.9%, while the 4 and 6% Ni alloys exhibit elongations of 0.9 and 0.8%, respectively, for the heat-treated condition.

A comparison of these results with those previously observed for similar PM steels in the quenched and tempered condition is shown in Table 3. Prior studies often do not differentiate between pre- and post-sintered carbon content, and it will be assumed that a pre-sintered carbon content of 0.5% in prior studies is comparable to the post-sintered 0.4% carbon

Table 3
A comparison of the present results with those obtained in prior studies

Study (alloy)	Density (g/cm³)	Tensile strength (MPa)	Elongation (%)	Bending fatigue strength at 106 cycles (MPa)	Processing and chemistry comments
Present (Fe–2Ni)–0.85Mo–0.4C	7.50	1530	1.9	373	DPDS
Narasimhan: [2] (Fe–1.8Ni)–0.5Mo–0.5C	7.20	1300	N/A	N/A	Lower density
Hanada: [7] (Fe–0.5Ni)–0.5Mo–0.5C	7.47	1711	N/A	N/A	Pre-alloyed powder
Hanada: [7] (Fe–2Ni)–1.0Mo–0.5C	7.50	1946	N/A	N/A	Diffusion bonded powder
Morioka: [7] (Fe–2Ni)–1.0Mo–0.6C	7.48	2000 approximately	N/A	420 approximately 10⁶ cycles	Diffusion bonded powder–higher C content
Furukimi: [6] (Fe–2Ni)–1.0Mo–0.6C	7.43	1920	N/A	N/A	Diffusion bonded powder–higher C content
Present (Fe–4Ni)–0.85Mo–0.4C	7.54	1551	0.9	395	DPDS
Hanada: [7] (Fe–4Ni)–1.5Cu–0.5Mo–0.5C	7.50	1203	N/A	N/A	Cu addition
Morioka: [8] (Fe–4Ni–1.5Cu–0.5Mo–O.6C	7.41	1700 approximately	N/A	350 approximately 10⁶ cycles	Cu addition–higher C content
Present (Fe–6Ni)–0.85Mo–0.4C	7.55	1579	0.8	361	DPDS
Narasimhan: [2] (Fe–6Ni)–0.85Mo–0.5C	7.42	1345	N/A	N/A	Warm compaction–lower density:
Narasimhan: [2] (Fe–6Ni)–1.5Mo–0.5C	7.42	1400	N/A	N/A	Warm compaction–lower density:

All results are in the quench-and-tempered condition, however, temper temperatures may vary. The last column in the table identifies a difference in processing compared to the present study that could significantly affect the results.
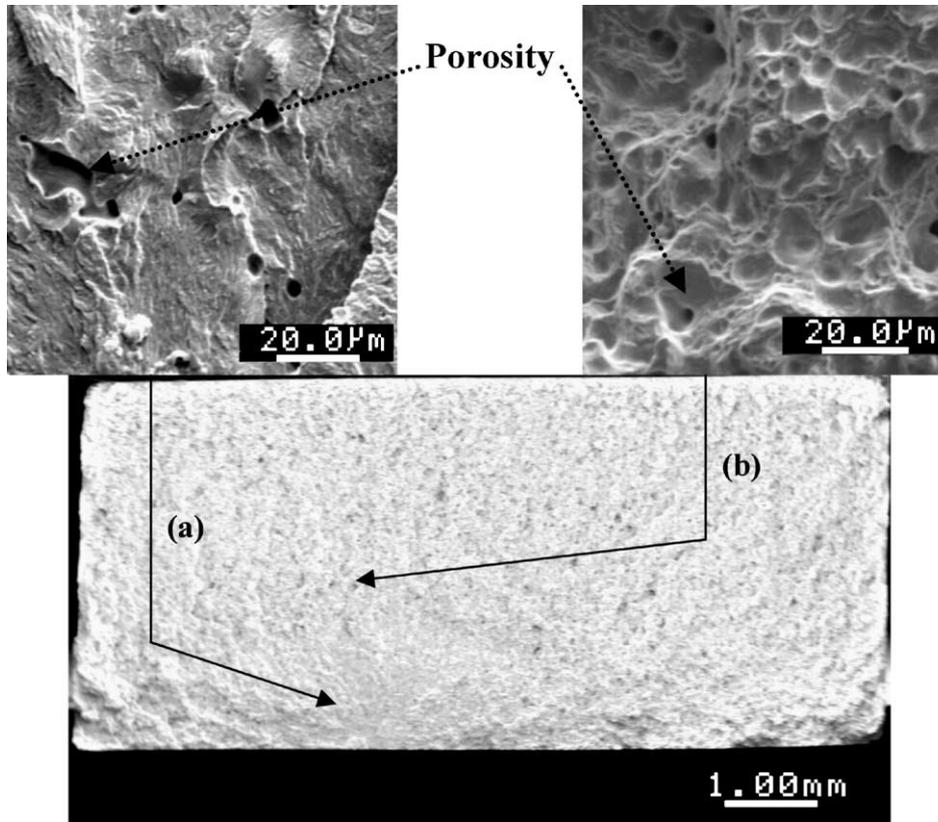
Fig. 3. SEM micrographs of fatigue specimen fracture surface, showing (a) ductile tensile fracture and (b) fatigue fracture regions. Porosity is indicated with dotted arrows.

content in the present study, as some decarburization during the sintering process is likely. Compared to previous studies at similar density levels [2,8,13], the 2% Ni alloy tested in this study had a lower strength. The primary reason for the lower strength was the use of elemental, admixed Ni as apposed to pre-alloyed or diffusion bonded Ni, resulting in soft (and larger) Ni-rich regions.

Another possible reason for the lower strength of this study is that the temper temperature of this study was 390 °C, which is the highest accepted tempering temperature for these alloys and is higher than most of the other studies. The 4% Ni alloy exhibits a strength that is mid-range in value when compared to previous studies. For example, the strength results of this study were higher in comparison to Hanada et al. [7] because Cu additions tend to decrease the "heat-treated" strength [6]. On the other hand, tensile strengths attained in this study were lower than those of Furukimi et al. at 2% Ni [6]. Cu additions were also present in the study of Furukimi and coworkers, but the carbon content was higher and the temper temperature was lower, which can result in higher strengths. For the 6% Ni alloy, no direct comparisons for DPDS are available, but other high density processing (i.e. warm compaction) was performed on 6% nickel steels [2]. The 6% Ni alloy of this study displayed a higher strength in comparison to the Narasimhan study [2], mainly due to higher density. The Narasimhan study offers a direct basis of comparison in

terms of alloying, because admixed Ni additions were made to the alloy, as was the case for the present study. In general, the results of this study are similar to previous results of similar studies; therefore, the fatigue data of the following section should also be representative of this class of P/M steels.

3.3. Mechanical properties: fatigue behavior

Fatigue tests were performed on the three alloys in the quenched and tempered conditions, and the results of the staircase tests appear in Table 2. In all cases, the ratio of fatigue strength to tensile strength was in the range of 0.23–0.25. The 4% Ni alloy shows the highest average fatigue strength of approximately 395 MPa, while the 2% Ni alloy exhibits intermediate fatigue strength of approximately 373 MPa. The 6% Ni alloy, which had the highest tensile strength and porosity level (Table 2), exhibited the lowest fatigue strength of 361 MPa. This behavior is consistent with other studies that show porosity in P/M alloys decreases fatigue strength significantly [21–23]. It should be noted that, given the scale of the standard deviations of the fatigue strengths, the differences between the fatigue strengths of the alloys are small.

The present fatigue results may be compared with those of Morioka, who examined a 2% Ni alloy with 0.6% C (as opposed to 0.4% C here) and processed using diffusion bonded

Table 4
Analysis of the projected pore content on the fracture surface of (Fe–2Ni) P/M steel, where both fatigue and ductile fracture modes were observed

Fracture surface	Approximate crack length (mm)	Porosity on fracture surface (%)	Ratio to bulk porosity
Fatigue crack region	0.5	11.4 ± 1.2	2.4 ± 0.3
Ductile fracture region	3.0	33.7 ± 0.6	7.2 ± 0.2

powders [8], rather than elemental Ni in our case. As shown in Table 3, while the 2% Ni alloy of this study has a lower fatigue strength, it exhibits a slightly higher fatigue strength to tensile strength ratio, 0.24, than that of Morioka who obtained a ratio of 0.21. For the 4% Ni alloy, the fatigue strength was higher than that found by Morioka. As with the 2% Ni alloy, the tensile strength to fatigue strength ratio was also higher, 0.25 compared to 0.21, respectively.

3.4. On the effects of porosity on tensile and fatigue properties

In this study, porosity has shown to decrease both tensile and fatigue strengths of the heat-treated P/M steels, as expected. To explore the influence of porosity on these different modes of fracture, the fracture surfaces were examined to determine the relative levels of porosity on the fatigue and tensile fracture surfaces. As shown in Fig. 3, the fracture surfaces of the quenched and tempered fatigue specimens were analyzed for projected area fraction of porosity, and the results are shown in Table 4.

Quantification of porosity was performed via image analysis by means similar to Danninger et al. [24], although fracture was not performed at low temperatures which would have prevented ductile deformation. Despite this fact, the sintered compacts showed little ductility and any miscalculation due to deformation can be reflected in the error reported with each value. The Dannigner study focused on the effective load bearing cross-section (A_c) of the fracture surface, which is a parameter used to predict tensile and fatigue strength of sintered compacts. The present study focuses on the pore content of the fracture surface and how it changes with crack growth phenomena. Surface porosity and A_c are direct opposites of each other.

The amount of porosity on the ductile tensile fracture surface is ≈7.2 times that of the bulk porosity or roughly one-third of the fracture surface as viewed in Fig. 3. In contrast, the area fraction of porosity on the fatigue fracture surface was much lower at ≈2.4 times the bulk porosity. The implication is that crack growth associated with tensile fracture follows a rough, irregular plane of high pore content. In contrast, fatigue crack growth is much less dependent on porosity, which is consistent with earlier observations that porosity has only a small effect on fatigue crack propagation rates [25]. Thus, the fracture surface of the fatigue crack region is less dependent on porosity and contains a smaller number of pores.

The higher degree of pore participation in tensile crack growth can be understood in terms of the relative scales of the crack-tip plastic zones when compared to the scale of the pore microstructure. In a tensile test, plasticity within the entire specimen gauge volume is the driving force; the eventual fracture path is one of high pore content and is tortuous and zigzagged in nature [26]. For crack growth processes, plasticity and damage is confined to the crack-tip plastic zone. For crack lengths in Table 4 and correcting for the differences between cyclic and monotonic plastic zone sizes, the plastic zone, r_p, will be approximately 24 times larger for the tensile fracture stage of crack growth than for the fatigue fracture portion [27]. Since damage is confined to a plane $\pm\ r_p$ of the main crack, only a comparatively small number of pores can participate in the fatigue crack growth process. In contrast, the tensile overload region, r_p, is large and pore participation in the tensile crack growth process is about 3 times greater (Table 4). As a result, the *fatigue* fracture surface is comparatively flat, as fewer pores cause crack deviation, and it also contains a lower fraction of porosity.

The effect of pore size on the fatigue strength was also investigated in this study. An analysis of the distribution of pore sizes shows that the 4% Ni steel, which had the highest fatigue strength (Table 2), also had the smallest percentage of pores larger than either $10\,\mu m$ or $20\,\mu m$. Thus, as has been observed in the influence of porosity on fatigue of castings, large pores can significantly reduce high cycle fatigue strength [28]. With the smallest fraction of large pores, the 4% Ni alloy will have the smallest likelihood to initiate a long fatigue crack, consistent with its highest fatigue strength.

4. Conclusions

The influence of Ni content (2,4, and 6 wt.% levels) on the microstructure and mechanical properties has been examined in a series of Fe–xNi–0.85Mo–0.4C steels fabricated by powder metallurgy using elemental Ni additions, relying on a double-press double-sinter processing route to increase density. The results indicate that in the *as-sintered condition* increasing nickel content increases tensile strength and decreases elongation to fracture as a result of increased levels of hard constituents (martensite and lower bainite) within the microstructure. In contrast, after the quench-and-temper heat treatment, Ni additions have no significant effect on tensile strength but decrease elongation slightly for the tempered martensitic structures. Fatigue results for quenched and tempered conditions indicate that the 4% Ni steel has the highest fatigue strength at 10^6 cycles, consistent with the lowest level of large (>$20\,\mu m$) pores in this case.

Acknowledgements

The authors wish to thank The Center for Innovative Sintered Products for supporting this effort under BFTDA Grant No. 21-116-0011. Insightful discussions with John Kosco of Keystone Powdered Metal Company, Edmond Ilia of Metaldyne Sintered Components, and Francois Chagnon of Quebec Metal Powders Limited are also acknowledged.

References

[1] Y. Bergstrom, L. Troive, Nord. Steel Min. Rev. 3 (1999) 126.

[2] K. Narassimhan, J. Tengzelius, Adv. Powder Metall. Part Mater. 5 (1992) 153.

[3] J. Hamill, R. Causton, O. Shuresh, Adv. Powder Metall. Part Mater. 5 (1992) 193.

[4] F. Gosselin, M. Gangne, Y. Trudel, Adv. Powder Metall. Part Mater. 5 (1992) 127.

[5] J. Kosko, in: W.B. Eisen, B.L. Ferguson, R.M. German, R. Iacocca, P.W. Lee, D. Madan, K. Moyer, H. Sanderow, Y. Trudel (Eds.), ASM Handbook: Powder Metal Technologies and Applications, vol. 07, Materials Park, OH, 1998. p. 751.

[6] O. Furukimi, K. Yano, S. Takajo, Adv. Powder Metall. 5 (1991) 59.

[7] M. Hanada, N. Motooka, T. Honda, Adv. Powder Metall. Part Mater. 5 (1992) 215.

[8] Y. Morioka, Met. Powder Rep. 45 (1990) 181.

[9] F. Hanejko, H. Rutz, U. Engstrom, B. Johansson, Adv. Powder Metall. Part Mater. 10 (1995) 77.

[10] H. Khorsand, H. Yoozhashizade, S.M. Habibi, K. Janghorban, A. Nangir, S. Reihani, Met. Powder Rep. 57 (2002) 32.

[11] J.J. Horn, R.I. Stephens, T. Prucher, Powder Metall. 41 (1998) 205.

[12] W.B. James, M.C. Baran, F.J. Semel, R.J. Causton, K.S. Narasimhan, Proceedings from Euro2000, Budapest, Hungary, July, 2000.

[13] A. Graham, T. Cimino, A. Rawlings, H. Rutz, Adv. Powder Metall. Part Mater. 13 (1997) 75.

[14] L. Pease, Int. J. Powder Metall. 37 (2001) 28.

[15] U. Engstrom, S. Allroth, Proceedings from Powder Metall. World Congress Part II, Dusseldorf, Germany, 1986, p. 1039.

[16] W. Jamesin, W.B. Eisen, B.L. Ferguson, R.M. German, R. Iacocca, P.W. Lee, D. Madan, K. Moyer, H. Sanderow, Y. Trudel (Eds.), ASM Handbook: Powder Metal Technologies and Applications, vol. 07, Materials Park, OH, 1998. p. 947.

[17] B. Gething, M.S. Thesis, Pennsylvania State University, University Park, PA, 2003.

[18] C. Lipson, N. Sheth, Statistical Design and Analysis of Engineering Experiments, McGraw-Hill, New York, 1973.

[19] L. Samuels, Optical Microscopy of Carbon Steels, ASM International, Metals Park, OH, 1980.

[20] F. Chagnon, Y. Trudel, Adv. Powder Metall. Part Mater. 5 (1995) 3.

[21] S. Polasik, N. Chawla, Proceedings from the 2002 International Conference on Powder Metallurgy and Paniculate Materials, Orlando, FL, June, 2002.

[22] T. Cimino, A. Graham, T. Murphy, Adv. Powder Metall. Part Mater. 13 (1998) 33.

[23] T. Cimino, A. Graham, T. Murphy, A. Lawley, Adv. Powder Metall. Part Mater. 7 (1999) 65.

[24] H. Danninger, U. Sonntag, B. Kuhnert, R. Ratzi, Prakt. Metallogr. 39 (2002) 8.

[25] R.A. Queeney, P.S. Dasgupta, Int. J. Fatigue 2 (1980) 113.

[26] H.J. Niu, I.T. Chang, Scr. Metall. 41 (1999) 481.

[27] S. Suresh, Fatigue of Materials, Cambridge Press, Cambridge, UK, 1991.

[28] Q.G. Wang, P.N. Crepeau, D. Gloria, S. Valtierra, Adv. Aluminum Cast. Tech. II (2002) 209.